Journal of The Electrochemical Society, **160** (2) A394-A403 (2013)
0013-4651/2013/160(2)/A394/10/$28.00 © The Electrochemical Society

Analysis of Electrochemical Lithiation and Delithiation Kinetics in Silicon

Vijay A. Sethuraman,[a,*,c,z] Venkat Srinivasan,[a,*,z] and John Newman[a,b,]**

[a]*Environmental Energy Technologies Division, Lawrence Berkeley National Laboratory, University of California, Berkeley, California 94720-1462, USA*
[b]*Department of Chemical and Biomolecular Engineering, University of California, Berkeley, California 94720-1462, USA*

Analysis of lithiation and delithiation kinetics in pulse-laser-deposited crystalline thin-film silicon (Si) electrodes is presented. Data from open-circuit relaxation experiments are used in conjunction with a model based on Tafel kinetics and double-layer capacitance to estimate the apparent transfer coefficients (α_a, α_c) and exchange current density to capacitance ratio (i_0/C_{dl}) for lithiation and delithiation reactions in a lithiated silicon (Li_xSi) system. Parameters estimated from data sets obtained during first-cycle amorphization of crystalline Si, as well as from cycled crystalline Si and amorphous Si thin-film electrodes do not show much variation, indicating that they are intrinsic to lithiation/delithiation in Si. A methodology to estimate the side-reaction rate on a well-cycled electrode and its role in the evolution of the open-circuit potential of the Li_xSi system are discussed. We conclude that the large potential offset between lithiation and delithiation reactions at any given state of charge is *partially* caused by a large kinetic resistance (i.e., small i_0). Using the estimated parameters, the model is shown to predict successfully the behavior of the system under galvanostatic lithiation and delithiation.
 [DOI: 10.1149/2.008303jes]

Manuscript submitted October 29, 2012; revised manuscript received December 6, 2012. Published December 28, 2012. This was Paper 607 presented at the Honolulu, Hawaii, Meeting of the Society, October 12–17, 2008.

Electrochemical lithiation and delithiation of silicon can be ideally represented as,

$$xLi^+ + Si + xe^- \leftrightarrow Li_xSi \quad [1]$$

The fully lithiated phase of silicon at room temperature is $Li_{3.75}Si$, which translates to a maximum theoretical capacity of 3579 mAh g^{-1} for silicon,[1] much higher than that of graphite (372 mAh g^{-1}).[2,3] When used in a lithium-ion battery, this high capacity results in a significant increase in the theoretical energy density and specific energy of the cell (by as much as 25 to 30% compared to existing graphite-based lithium-ion cells) and could help lower the cost per kWh. This high capacity combined with silicon's low discharge potential makes it an attractive choice for use as negative electrodes in lithium ion batteries. However, the large first-cycle capacity loss, continuously occurring side reactions during cycling, and the large volume change (ca. 300%) have all been detrimental to the commercialization of this system.[4] The electrochemical lithiation and delithiation of silicon at ambient temperatures have been extensively studied in recent years in such forms as nanowires,[5–7] amorphous thin films,[8–12] crystalline thin films,[13] crystalline powder,[14,15] composites,[16,17] and mixtures with carbon.[18–20] The above-mentioned detrimental characteristics appear in all of these studies. Reference 21 reviews the methodologies adopted for reducing the capacity loss observed in silicon anodes and the challenges that remain in using silicon and silicon-based anodes.

While much progress has been made in understanding the means of enabling Si anodes to cycle reversibly, one interesting feature of this electrode is the potential offset that exists between charge and discharge. The lithiation potential for a given state of charge is considerably lower than the delithiation potential at that state of charge (SOC). Furthermore, the difference between lithiation and delithiation potentials at a given SOC, defined as the potential offset, appears to be nearly rate independent.,[5,22] For example, even at low rates (i.e., C/10), the potential vs. Li/Li^+ during lithiation is lower than during delithiation by approximately 320 mV.[23] Furthermore, data in the literature seem to indicate that particle size[24] and film thickness[25] *may* have an effect on the potential offset, which varies from as high as 300 mV for composite electrodes[1] to less than 250 mV for nanowires[5] and amorphous thin-film electrodes.[25] As a consequence of this potential offset, the silicon electrode exhibits a stable hysteresis loop (as in a potential vs. capacity plot) at every SOC upon lithiation and delithiation. Similar to nickel hydroxide,[36] a hysteresis loop created during a complete lithiation and delithiation cycle is not sufficient to define the state of the Li_xSi system, even at low rates. Also, the potential obtained at any SOC depends on the cycling history of the Li_xSi system and therefore cannot be used as an indication of the SOC of the cell. This potential offset also results in lowering the cell efficiency (e.g., 91.5% cell energy efficiency at low rates when paired with a 3.8 V $LiNi_{0.8}Co_{0.15}Al_{0.05}O_2$ cathode).

There are several documented examples of potential hysteresis in electrochemical systems such as the NiOOH electrode,[36] carbon nanotubes,[37–39] bulk graphite,[40–43] Li_xWO_3,[44] $Li_{1\pm y}NiO_2$,[45] $Pr_{0.7}Ca_{0.3}MnO_3$,[46,47] $LiMnO_2$,[48–50] $LiMoN_2$,[51] $Li_{3-y}V_2(PO_4)_3$,[52] $Li_ySiSnON$,[53] $LiFePO_4$,[54,55] Si-Sn alloys,[56] Si-C-O,[57] certain conducting polymers[58] such as α-phenylenes, α-thiophenes,[59] polypyrrole,[60] and polyaniline,[61,62] $La_{0.9}Sr_{0.1}MnO_3$/YSZ,[63,64] PEM fuel cells,[65] and certain redox proteins.[66] There is no single reason given as to why potential hysteresis occurs in all of these systems – for example, potential hysteresis upon lithium intercalation and deintercalation in hydrogen containing carbons was attributed to lithium binding on hydrogen terminated edges of hexagonal carbon fragments resulting in an sp^2 to sp^3 bond transition.[40] A simple model which accounts for the energy associated with this bonding change was able to predict the observed potential hysteresis.[67] This Arrhenius-type model also predicts a decrease in potential offset by 59.8 mV for every order of magnitude change in discharge rate, which suggests that the phenomenon is reversible (i.e., the potential offset is rate dependent). On the other hand, in systems exhibiting phase transitions upon lithium insertion and de-insertion such as $LiMnO_2$, the potential hysteresis is thought to be caused by domain-like microstructures with spinel embedded in layered material.[48]

Potential hysteresis exhibited by amorphous Si-Sn alloys, the closest to the system studied in this work, upon lithiation and delithiation is thought to occur by differences in energy dissipated during the changes in the local atomic environment around the host atoms and lithium.[56] Neudecker et al.[53] measured the open-circuit potential relaxation from the lithiation and delithiation curves for various phases in a $Li_xSiSnON$ electrode in a solid-state battery (i.e., without a liquid electrolyte) and found that the potentials were evolving at an extremely slow pace. They fit the potential relaxation to logarithmic time dependence and, extrapolating to 10 years, still obtained a potential offset of approximately 100 mV between the lithiation and delithiation profiles. Because of this, they attribute this behavior to a true thermodynamic hysteresis and argued that the origin for this

*Electrochemical Society Active Member.
**Electrochemical Society Fellow.
[c]Present address: School of Engineering, Brown University, Providence, Rhode Island 02912, USA.
[z]E-mail: vj@cal.berkeley.edu; VSrinivasan@lbl.gov

could be the presence of metastable domains in the electrode which are sensitive to the direction of lithium transfer.[53] Similar behavior was also observed in amorphous $Li_xMn_{2-y}O_4$ cathodes, also thought to be caused by metastable domains.[50] Although potential hysteresis in electrochemical systems resembles those exhibited by ferroelectric hysteresis, the difference lies in compositional inhomogeneity typically seen in the former. One of the objectives of this study is to understand, quantify, and describe mathematically this potential offset seen in the silicon electrode.

We have recently measured in situ the stresses generated in the silicon thin-film electrode during lithiation/delithiation, and shown that ca. 40% of the energy loss (between lithiation and delithiation) can be accounted for by mechanical dissipation.[68–70] However, the origin of the rest of the potential offset remains indeterminate. In this paper, we postulate that the Li_xSi system is kinetically limited at practical lithiation and delithiation rates (i.e., C/30 to 3C), and that a small exchange current density (i_0) causes the observed phenomena. As a result, the open-circuit-potential relaxation is slow and takes a long time to reach equilibrium. The objective of this study is to explain quantitatively the electrochemical behavior of the silicon electrodes during lithiation and delithiation and to check the above-mentioned postulate. Inherent in these objectives lie answers to the following questions: (i) What causes the potential offset between lithiation and delithiation in this system, and how does this potential offset behave under various electrochemical conditions? (ii) What parameters characterize this offset, and how can they be extracted quantitatively? (iii) Can the extracted parameters then be used in conjunction with a continuum model to predict the electrochemical behavior of the system? and (iv) Can this potential offset be eliminated? These objectives were accomplished by a series of cycling and open-circuit relaxation experiments on a pulse-laser-deposited (PLD) thin-film silicon electrode in conjunction with a kinetic model based on Tafel kinetics with double-layer charging with and without the side reaction (i.e., electrolyte reduction). The PLD silicon electrode was chosen as a model system because it behaves like a composite electrode made with crystalline Si nanoparticles without presenting the mathematical complexities from a distributed reaction. In addition, thin-film Si electrodes exhibit minimal capacity fade and are reversible for a moderate number of cycles. In the first part of this study, the quasi-equilibrium potential was measured as a function of SOC from a series of open-circuit relaxation experiments on a fresh silicon electrode (i.e., initial lithiation/delithiation resulting in amorphization) as well as on a well-cycled electrode. The data collected from these relaxation experiments were used to estimate the apparent transfer coefficients and the ratio of exchange current density to double-layer capacitance for lithiation and delithiation reactions as a function of SOC. These kinetic parameters were then used to predict the lithiation and delithiation potential profiles. The model results prove our initial hypothesis and give insights into the origin of potential offset and ways to eliminate this potential offset.

Experimental

Substrate preparation.— 1.2-mm-thick stainless steel disks (diameter = 1.8 cm) were successively wet polished with 140, 75, 23, and 12.5 μm silicon carbide abrasive papers (Leco Corp., St. Joseph, MI) and cleaned successively in ultrasonic baths of acetone, methanol, and de-ionized water for 15 minutes each. The substrates were then attached to a substrate holder in a home-built pulse-laser deposition chamber such that the polished surface was facing the plume. The distance between the substrate and the target was 5 cm.

Electrode preparation.— Cu and Si thin films were deposited at room temperature (ca. 23°C) in an argon atmosphere with a pressure of 66.7 Pa. Before deposition, the chamber was pumped down to a base pressure of 2.66×10^{-5} Pa. A pulsed krypton-fluoride (KrF) excimer laser ($\lambda = 248$ nm, Lambda Physik LPX 210i) was focused onto the targets. Pure copper and silicon (99.999%, Super Conductor Materials, Inc.) targets were used to deposit copper and silicon respectively. The energy flux on the target was approximately 2.4 J/cm^2, and the incident angle between the laser beam and the target normal was 45 degrees. The pulse frequency was 10 Hz, and the pulse duration was 25 ns. A layer of copper was deposited followed by a layer of silicon. The copper underlayer provides better film adhesion, as shown by Maranchi et al.[71] and by Sethuraman et al.,[72] and without this layer the cell did not cycle very well. The respective deposition times were 14 and 180 minutes.

Electrode characterization.— The pulse-laser-deposited (PLD) sample was examined in a high-resolution JEOL JSM-6340F field-emission scanning electron microscope operated at an accelerating potential of 5 kV using 5 mm as the working distance with the secondary and backscattered electron-image detectors. Energy dispersive X-ray (EDX) spectroscopy was carried out using a Genesis XM2 microanalysis system (EDAX Inc., Mahwah, NJ) to evaluate the composition of the film. The surface was also analyzed by Raman microscopy (Labram, ISA Groupe Horiba) with a helium-neon (HeNe) laser ($\lambda = 632.8$ nm) at 1 mW power as the excitation source. The electrode was then assembled into a coin cell configuration (#2325, i.e., 23 mm diameter and 2.5 mm total thickness) obtained from the National Research Council (NRC, Canada) with a lithium metal counter and reference electrode (diameter = 1.5 cm) and a woven Celgard 2500 separator (diameter = 1.9 cm, thickness = 21 μm, Celgard Inc., Charlotte, NC). 1.2 M lithium hexafluoro phosphate in 1:2 (vol.%) ethylene carbonate/diethyl carbonate (Ferro Corporation, Independence, OH) was used as the electrolyte.

Electrochemical measurements were conducted in an environmental chamber at 25°C (±1°C) using a Solartron 1480A MultiStat system (Solartron Analytical, Oak Ridge, TN), and data acquisition was done using Corrware (version 2.8d, Scribner Associates Inc., Southern Pines, NC). The cell was cycled galvanostatically at ca. 20 μA/cm^2 between 1.2 and 0.01 V vs. Li/Li$^+$. The data acquisition rate was 1 Hz for all the electrochemical experiments. Rate experiments (from C/30 to C/4) were conducted galvanostatically between an upper cut-off potential of 1.2 V vs. Li/Li$^+$ and 50% SOC. This lower limit was chosen to avoid lithium plating and also to avoid the formation of the crystalline $Li_{22}Si_5$ phase.[1,14] Cycling data obtained on a well-cycled electrode (as potential vs. charge) were corrected for parasitic side reactions and normalized from z = 0 to 1 (where z is state of charge). Open-circuit relaxation experiments were conducted as a function of SOC at ca. 16% intervals. The input impedance of the instrument was 12 GΩ. Since the impedance of the coin-cells used in this study was significantly lower than this value, the error due to the open-circuit-potential measurement was negligible.

Results and Discussion

Figure 1 shows the surface morphology of the pulse-laser deposited (PLD) silicon film. The film exhibits a highly cracked surface with a grain-size distribution centered approximately on 140 nm and appears to be porous. The presence of bigger chunks of silicon on the surface is due to the randomness of the laser ablation of the silicon target and is typical of PLD films.[73] The mean-crystallite size distribution in these PLD films is similar to that of Si particles used to fabricate composite electrodes.[14] A detailed study on the properties of PLD silicon thin films deposited using a KrF excimer laser can be found in the study reported by Chen et al.[73] The elemental X-ray analysis of the PLD film (not shown) indicates that the surface is predominantly silicon. The Raman spectrum (shown in Figure 2) obtained on the PLD silicon thin film is identical to that from a boron-doped Si (100) wafer with a sharp peak at 521 cm^{-1} and is therefore highly crystalline. The mass of the film was not measured, and therefore the capacity of the film is either normalized to the maximum capacity obtained or expressed as charge (in A · s units) throughout this article.

Film behavior.— Figure 3 shows the potential curves of the PLD silicon thin-film electrode cycled at C/8 rate ($I_{app} = \pm 20.68$ μA/cm^2)

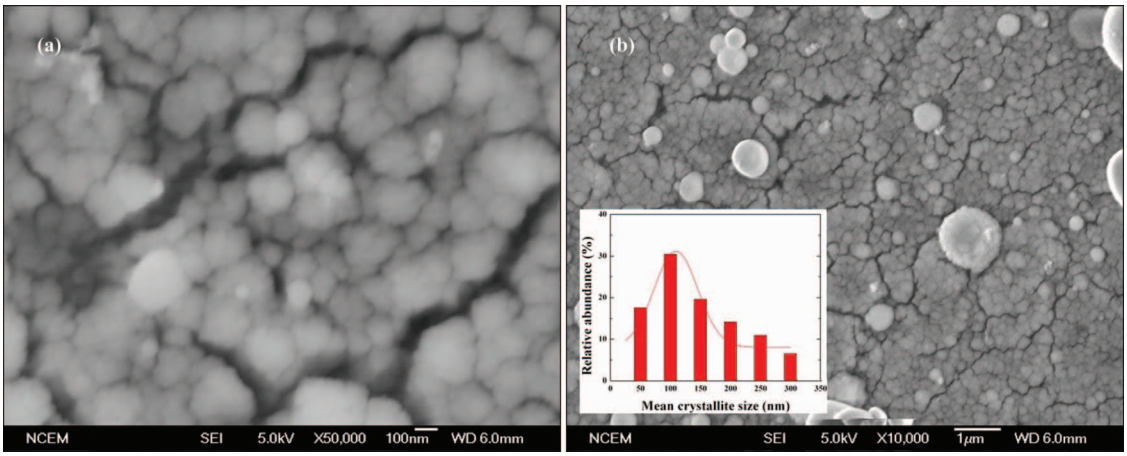

Figure 1. Scanning electron micrographs of a pulsed-laser-deposited silicon film. The inset shows the histogram of mean crystallite size estimated from the image on the left. The scale bar on the left is 100 nm, and that on the right is 1 μm.

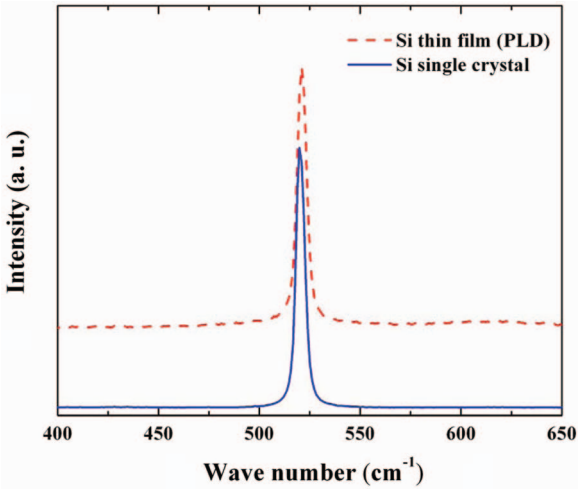

Figure 2. Raman spectrum obtained on a pulse-laser-deposited Si thin film is compared to that of a single-crystal (100) Si wafer. Spectra are shifted arbitrarily up the intensity axis for clarity. The peak at 521 cm^{-1} is characteristic of a highly crystalline Si.

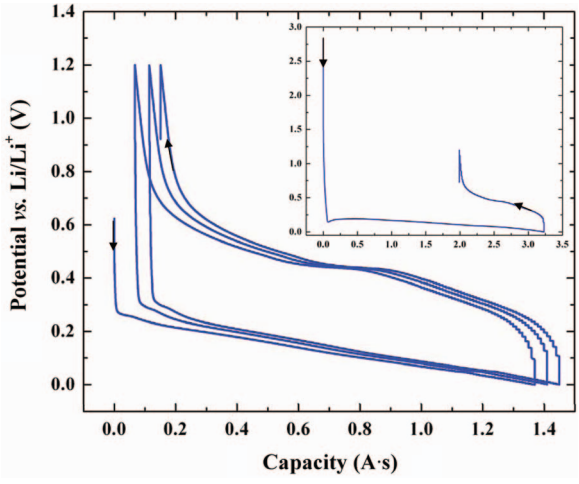

Figure 3. Cell potential vs. capacity curves corresponding to lithiation and delithiation of pulse-laser-deposited Si thin-film electrode cycled at C/8 rate between 1.2 and 0.01 V vs. Li/Li+. These curves were obtained on a well-cycled cell. Inset: Cell potential vs. capacity curves corresponding to the first lithiation and delithiation of the same electrode.

between 1.2 and 0.01 V vs. Li/Li$^+$. These curves were obtained on a cell that had reached steady-state cycling efficiency (ca. 5 cycles). The cycling behavior of the PLD Si thin film is very similar to that of an undoped single-crystal Si[74] and a composite electrode made with crystalline silicon powder.[14] The potential during the initial lithiation (shown in Figure 3 inset) is relatively capacity-invariant due to solid-state amorphization of the crystalline Si thin film, and the corresponding first-cycle irreversible capacity loss is approximately 60%. The potential offset between charge and discharge was 320 mV at 50% SOC after five lithiation-delithiation cycles. The steady-state lithiation capacity was higher than that of the delithiation capacity by approximately 1.8%. Although there was no evidence for the formation of the crystalline $Li_{3.75}Si$ phase during lithiation below 50 mV vs. Li/Li$^+$, the delithiation potential profile also exhibits a characteristic flat plateau in the neighborhood of 50% SOC. Based on literature data and from the sloping potential profile, we believe we are cycling in the amorphous region. Figure 4 shows the lithiation and delithiation capacities for the first five cycles. Similar to other forms of silicon electrodes reported in the literature, the PLD silicon exhibits a large irreversible capacity loss during the first cycle (ca. 60%), and the cycling efficiency goes up above 98% for the subsequent cycles, evidence of side reactions contributing to the loss in efficiency. The large surface-to-volume ratio typical of highly cracked thin films provides

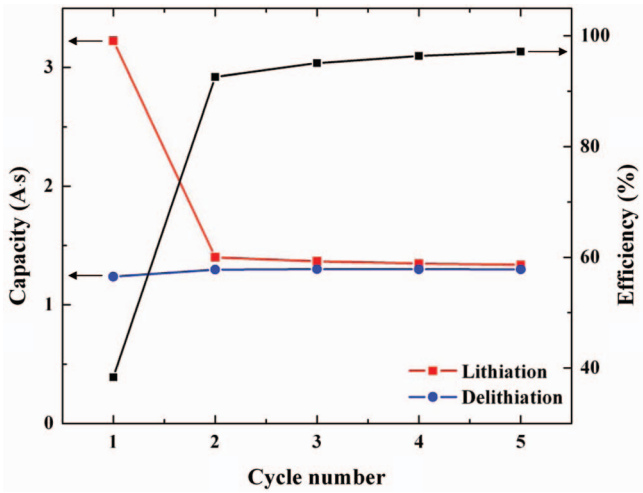

Figure 4. Lithiation and delithiation capacities for the first five cycles shown along with the respective cycling efficiency. The experiments were conducted at C/8 rate.

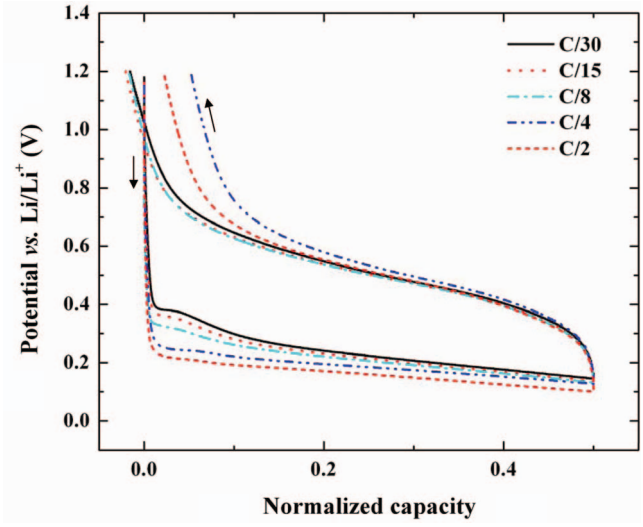

Figure 5. Cell potential vs. capacity curves for different lithiation and delithiation rates (from C/30 to C/2) cycled between 0 and 50% SOC. The electrode was cycled 10 times before conducting the experiment.

a large area for electrolyte reduction and solid-electrolyte-interphase (SEI) layer formation for a given electrode capacity.

Figure 5 shows data obtained between 0 and 50% SOC for different lithiation and delithiation rates (from C/30 to C/2) on this cell. It can be seen that the cycling rate has very little impact on the potential offset between lithiation and delithiation, similar to the rate capability data reported on Si nanowires[5] and amorphous Si thin films.[22] Sometimes, for a given SOC, a potential that is invariant with current-density is taken to be indicative of a system that is operating at or very near thermodynamic equilibrium. If this were true, the data in Figure 5 would suggest that the Si electrode exhibits two equilibrium potentials for every SOC, one on lithiation and one during delithiation. We test the nature of these potentials by performing potential-relaxation experiments (Figure 6) which shows the relaxation of cell potential at open circuit at 50% SOC after lithiation and delithiation at a C/8 rate.

The open-circuit potential corresponding to delithiation (the curve on the top) decreases rapidly at first (<2 hours), levels out (from 2 to 10 hours), and then increases slowly (>10 hours). On the other hand,

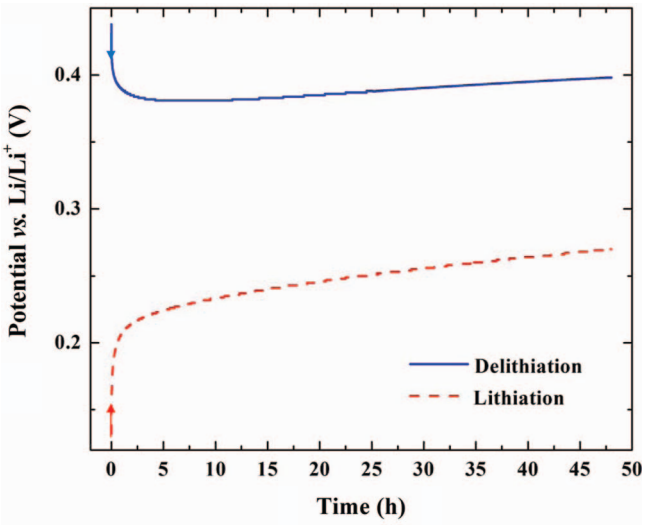

Figure 6. Relaxation of open-circuit potential (data) at 50% SOC during delithiation (upper curve) and lithiation (lower curve). The potential was changing even after 48 hours.

the open-circuit potential corresponding to lithiation (the curve in the bottom) increases more rapidly at first (<2 hours) and then evolves more slowly (>2 hours). Firstly, this indicates that the closed-circuit potential (i.e., under galvanostatic conditions) is not the equilibrium potential for this system. Secondly, the fact that both curves evolve slowly toward a higher value at longer times indicates the presence of a unknown side reaction with a higher equilibrium potential, which makes it difficult for the potentials to collapse onto an equilibrium value for this SOC. The presence of the side reaction is not surprising considering the large overpotential for the solvent reduction reaction at these potentials. A large body of work exists in the literature on this solvent reduction reaction as well as on the surface chemistry and morphology of the SEI layer.[26–33] These studies suggest that the SEI layer is unstable because of the large volume changes associated with lithiation and delithiation of Si electrodes, and continuous reformation of this layer occurs whenever new electronically conducting surfaces become available for solvent reduction.[34,35] Further progress in estimating the true SOC in this system requires a methodology to account for the side reaction. We perform this correction in a manner similar to that shown in previous studies,[36,75,76] as described below.

Side-reaction correction.— If the marching behavior seen from cycle to cycle (e.g., in Figure 3 for a cell that has reached steady cycling) is caused by the electrolyte reduction reaction, the applied current during the lithiation process can then be written (ignoring double-layer charging) as:

$$\text{Total current}\left(i_{app}\right) = \text{Lithiation current}\left(i_{main}\right) + \text{Electrolyte reduction current}\left(i_{side}\right) \quad [2]$$

Similar to the approaches taken by Darling and Newman[75] for the $Li_yMn_2O_4$ system and by Ta and Newman[76] for the nickel hydroxide system, we assume Tafel kinetics for the electrolyte-reduction reaction. The current due to this reaction can be written as,

$$i_{side} = -i_{0,side}\exp\left[-\frac{\alpha_{side}F}{RT}\left(V - U_{side}\right)\right] \quad [3]$$

The transfer coefficient for the side reaction, α_{side}, was assumed to be 0.5. While Tafel kinetics does not provide an explicit equilibrium potential (i_o and U are related), we assume a value of U_{side} = 0.8 vs. Li/Li$^+$ to estimate i_0. This side-reaction current was then calculated through the cycle assuming an i_0 such that the marching was eliminated from the cycling data. This is illustrated in Figures 7a and 7b. Figure 7a shows the steady state cycling data (obtained after the cell had reached a stable delithiation capacity) comprising of five lithiation/delithiation cycles. When the correction described above is performed, the curves collapse on top of each other as evidenced in the data in Figure 7b. The rate constant, i_0, estimated from this procedure was 7.5×10^{-13} A/cm^2, based on the cross-sectional area. Using the extracted kinetic parameters, the true SOC of the system can be determined under various conditions by correcting for the side reactions. The accuracy of this estimation procedure can be improved with increasing the number of lithiation/delithiation cycles that are simultaneously used to eliminate the marching behavior. Correcting the cycling data for side reactions using this approach can only be performed a well-cycled electrode, where the cycle-to-cycle capacity remains constant, and not on a fresh electrode (i.e., during the initial lithiation/delithiation cycles) where irreversible loss in capacity occurs due to reasons other than the electrolyte reduction reaction alone.

Equilibrium potential of the Si electrode.— Figure 8 shows the open-circuit potential after 10-hour relaxation period for lithiation and delithiation as a function of SOC. The figure shows that, similar to what is described above, the potential relaxes to a lower value from the lithiation curves compared to the delithiation curve, at the same SOC. Close examination of the data shows that the potential relaxes to 60% of the way toward the dashed equilibrium line. Complete potential relaxation is not achieved even on longer open-circuit times,

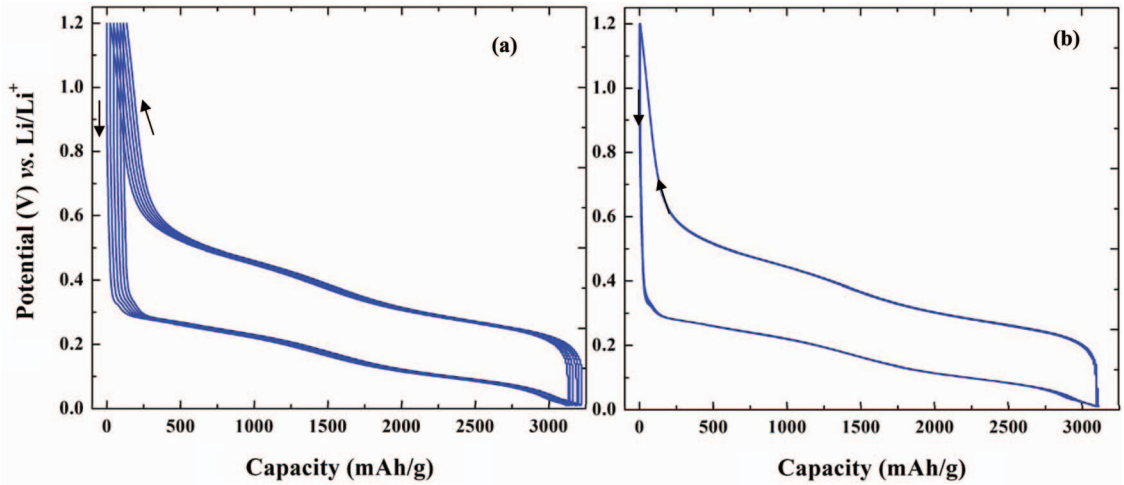

Figure 7. Cell potential vs. capacity curves for five lithiation/delithiation cycles of a pulse-laser-deposited Si thin-film electrode cycled at a C/8 rate between 1.2 and 0.01 *V* vs. Li/Li+ shown in (a) is corrected for the side reaction, and the result is shown in (b). Note that these curves were obtained after the cell had reached a steady-cycling condition.

and is essentially complicated by the presence of the side reaction, leading to the self-discharge (i.e., self delithiation) of the electrode (as shown in Figure 6). As mentioned earlier, in our studies on stress effects in thin-film geometry,[68,69] 40% of the energy lost between charge and discharge is accounted for due to mechanical dissipation. We note that the potential drop between the lines and the symbols in Figure 8 at 50% SOC account for 60% of the energy loss. The correlation between these numbers suggests that stress has a role in the potentials measured in this figure. Understanding the impact of stress and mechanical dissipation on the chemical potential of silicon would require a much more detailed study of this system, which is outside the scope of this paper.

Figures 6 and 8 suggest that achieving a true equilibrium value at a given SOC would require relaxation to very long times; longer than the relaxation times reported here. However, the presence of the side reaction results in the self-discharge of the electrode continuously, further complicating this estimation. A methodology similar to the one described above has been used in the past to estimate an equilibrium potential when a side reaction is present.[36,75,76] References 36 and 76 are very similar to the present system in that the chemistry studied by these authors (the NiOOH electrode) also exhibits a potential hysteresis. However, in both these papers the authors were studying a system that was thought truly to have multiple potentials at the same SOC, and therefore no attempt was made to estimate a single equilibrium potential from the data. The Si system is similar to the NiOOH system in that the closed-circuit potential does not appear to represent the equilibrium potential, suggesting that the equilibrium potential at any given state-of-charge lies somewhere between the close-circuit potentials. Estimating an equilibrium potential for Li insertion in Si has been a subject of previous study by Chevrier and Dahn,[77] who used density functional theory to estimate this potential and show a single equilibrium potential vs. composition curve between the closed-circuit potentials. They argue that the breaking of Si bonds causes the hysteresis in potential during closed-circuit conditions. On the other hand, Baggetto et al. reported two equilibrium curves *versus* SOC, one each for lithiation and delithiation, using a galvanostatic-intermittent-titration technique (GITT).[79] The authors argue that the two equilibrium potentials for a given SOC suggest two material states; however no proof is provided for this conclusion. Chandrasekaran et al.[80] also use two different equilibrium potentials for any given state of charge to model separately the lithiation and delithiation processes at room temperature. In other words, the symbols shown in Figure 8 are equivalent to equilibrium values reported by Baggetto et al.[79] and Chandrasekaran et al.[80] which would indicate the existence of path dependence in this system. As described above, the relaxation of potential in Si is a very slow process, and estimating the potential from a GITT is not straightforward when there is a significant side reaction present or even without the side reaction but with the very low value of i_0.

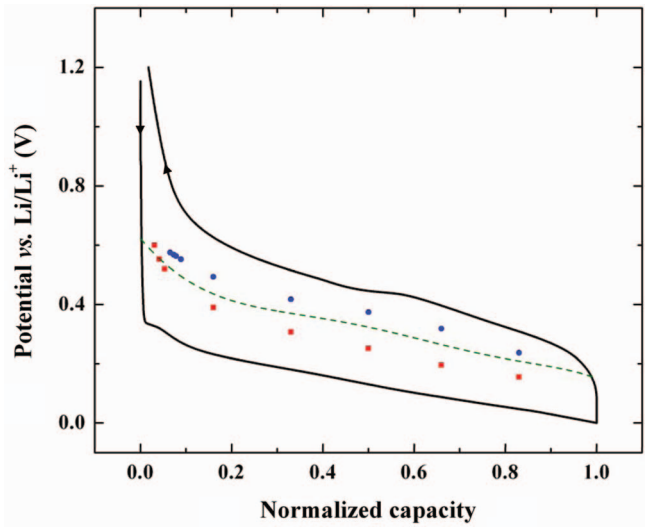

Figure 8. Open-circuit potential at the end of a ten-hour relaxation experiment during lithiation (-■-) and delithiation (-●-) experiments as a function of SOC. The solid line corresponds to a lithiation/delithiation experiment between 1.2 and 0.01 V vs. Li/Li+ at a constant current density corresponding to C/8, and the dashed line represents the potential used for model simulations (see text for details).

Parameter estimation from open-circuit-relaxation data.— The kinetic parameters for the Li_xSi system were estimated using data obtained from the open-circuit-relaxation experiments. In the mathematical treatment of the system, porous-electrode effects were ignored due to the use of a very thin film (thickness ≈ 300 nm) and the current small enough to ignore diffusion losses. For example, for diffusion coefficient values of 10^{-8} cm^2/s reported by Yoshimura et al.[81] and 5.1×10^{-12} cm^2/s reported by Ding et al.,[82] the respective time constants are 90 ms and 176 s, which are small compared to the hours associated with potential relaxation seen in this system.

Similar to the approach taken by Davis et al.[83,84] to model the behavior of the Li-CF_x system, the open-circuit potential relaxation

due to the main and side reactions driven by double-layer capacitance can be written as,

$$-C_{dl}\frac{dV}{dt} = i_0\left\{\exp\left[\frac{\alpha_a F}{RT}(V-U)\right] - \exp\left[-\frac{\alpha_c F}{RT}(V-U)\right]\right\} - i_{0,side} \times \exp\left[-\frac{\alpha_{side} F}{RT}(V-U_{side})\right] \quad [4]$$

The dependence of electrode stress on the kinetics of electrochemical lithiation and delithiation is ignored in writing this expression. Equation 4 is general and is used for relaxation after both lithiation and delithiation. We now describe the nature of the curve quantitatively. For the lithiation reaction, assuming Tafel kinetics, for a case without a side reaction, the analytic solution for Equation 4 is

$$V = U + \frac{RT}{\alpha_c F}\ln\left\{\frac{\alpha_c F i_0}{RTC_{dl}}t + \exp\left[\frac{\alpha_c F}{RT}(V_0 - U)\right]\right\} \quad [5]$$

where V_0 is the initial potential and U is the equilibrium potential, estimated as described above. At long times, this equation reduces to,

$$\frac{dV}{d\ln t} = \frac{RT}{\alpha_c F} \quad [6]$$

corresponding to a straight line in a plot of V vs. ln(t). Such behavior has been shown to be exhibited by the lead acid system,[85] Li-CF_x system,[83,84] and electrochemical capacitors and is considered a characteristic of a system that is limited by Tafel kinetics and a double-layer capacity.[86]

The equations above can be rearranged as shown by Davis et al. in dimensionless form to yield two dimensionless parameters, one that involves α_c and the second that combines i_0 and U. The rearrangement highlights the fact that in Tafel kinetics i_0 and U are coupled and cannot be independently determined. However, for the Li_xSi system in contrast to the CF_x system, which is irreversible, experiments can trace all the way around the lithiation/delithiation cycles, as in Figures 3, 5, and 7, etc., and both i_0 and U are needed, even if i_0 is quite small. This gives us a nice opportunity to explore apparent hysteresis in a system where both experiments and modeling are possible. Therefore, both of these quantities are reported in this paper.

In this paper we take the equilibrium to be a single potential curve between the closed-circuit potentials. This is shown as a dashed line in Figure 8 and is obtained by extrapolating the potential evolutions on open circuit. Note that this choice of the potential function has uncertainty but can be substantiated by comparisons of predictions with the results of experiments at open and/or closed circuit. This potential as a function of SOC was fit to a polynomial, shown in Figure 8 and given by

$$U = -4.76z^6 + 9.34z^5 - 1.8z^4 - 7.13z^3 + 5.8z^2 - 1.94z + 0.62, \quad 0 \le z \le 1 \quad [7]$$

The potential in the vicinity of $z = 0$ in Figure 8 is an extrapolation and is not the direct result of the open-circuit relaxation experiments. Note that this equilibrium curve differs from that of Chevrier and Dahn,[77] who calculate the equilibrium potential for a given SOC from the corresponding formation energies. In their potential vs. composition curve, the equilibrium potential increases sharply at very low SOCs (i.e., $0 < z < 0.02$) and decreases sharply at very high SOCs (i.e., $0.95 < z < 1$).

Using the U reported here, the values for the apparent transfer coefficients (α_a, α_c) and the ratio of the exchange current density to the double-layer capacitance (i_0/C_{dl}) were estimated by fitting Equation 5 with the experimental data. The data fits were obtained using a Levenberg-Marquardt[87] algorithm to minimize the sum of square of the error between the model prediction and the experimental data. Figure 9 shows the result for one such parameter-estimation procedure corresponding to open-circuit relaxation at 83% SOC after lithiation. The data yield $i_0/C_{dl} = 8.64$nV/s and $\alpha_c = 2.06$. Model fits with and without the side reaction are shown. The latter was the result of the analytic solution in Equation 5 (shown solid), and the former was

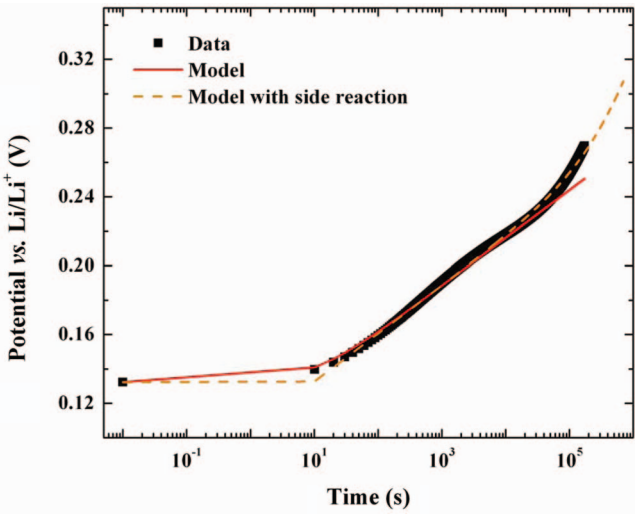

Figure 9. Relaxation of cell potential recorded at open circuit compared with model fits with and without side reaction. The symbols correspond to open-circuit potential data (-■-) at 83% SOC after lithiation; the solid and the dashed lines respectively correspond to Marquardt-Levenberg fits with and without side reactions.

the result of numerical solution to Equation 4 (shown dashed). The simulation shows that at times less than 5×10^4 s the two simulations yield identical results, while deviations start to occur beyond this point. While the model with the side reaction shows a change in the Tafel slope, the model without the side reaction does not show this change. The side reaction tends to pull the relaxation potential up (a reduction reaction) as shown in Figure 6, and fits the data better at times greater than 5×10^4 s.

This rise in slope of the potential-ln(t) curve at large times can be further understood by looking at the simulated current density for the main and side reactions on open circuit, as shown in Figure 10. When the electrode is operating at open circuit, double-layer discharge and both reactions occur simultaneously. The model predictions show that at short times (less than 5×10^4 s) the main reaction dominates while the side reaction component is lower, a consequence of the kinetics of the two reactions. However, as the potential of the electrode rises, the current for the main reaction starts to decease until its magnitude

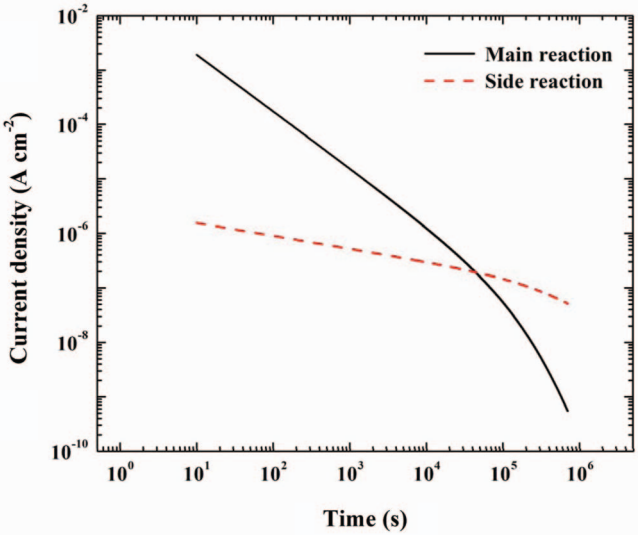

Figure 10. Estimated main-reaction and side-reaction currents during open-circuit potential relaxation at 83% SOC after lithiation.

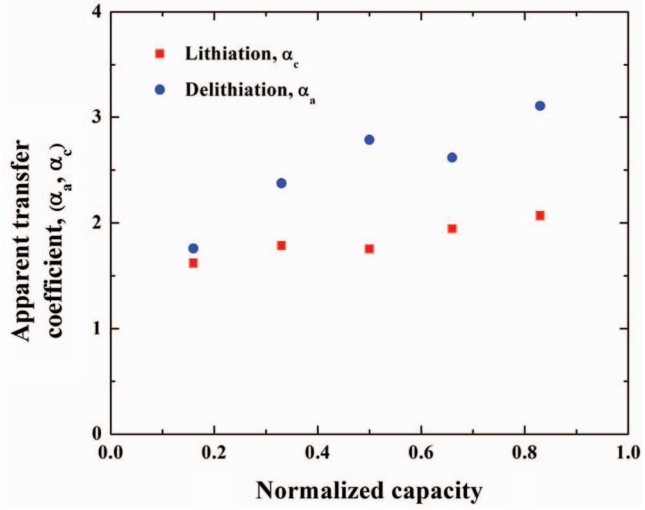

Figure 11. Apparent transfer coefficients for delithiation (αa, -●-) and lithiation (αc, -■-) reactions at various SOCs estimated from the open-circuit-potential-relaxation experiments.

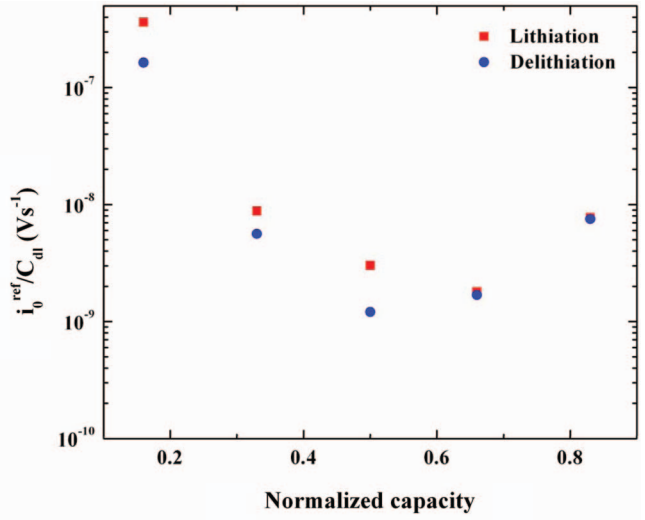

Figure 12. Values for i_0^{ref}/C_{dl} corresponding to lithiation (-■-) and delithiation (-●-) reactions at various SOCs estimated from the open-circuit-potential-relaxation experiments.

is lower than that for the side reaction. Beyond this point, the side reaction dominates the electrode's behavior. Open-circuit experiments that are conducted for longer times will lead to the self discharge of the electrode until the potential reaches the equilibrium potential of the side reaction (ca. 0.8 V vs. Li/Li^+) whose rate then becomes negligible. The change in the Tafel slope observed in Figure 9 provides a means of estimating the apparent transfer coefficient for the side reaction. However, this avenue was not pursued in this paper, and the value was assumed to be 0.5.

The method outlined above was used to estimate the apparent transfer coefficients (α_a, α_c) and the ratio of the exchange current density to the double-layer capacitance (i_0/C_{dl}) for various SOC for the main reaction. The exchange current density can be further split to eliminate the activity coefficient dependence by using the expression,[78]

$$i_0 = i_0^{ref}(z)(1-z)\frac{dU}{dz} \quad [8]$$

The coefficient i_0^{ref} refers to the rate constant for the lithiation or delithiation reaction without the dependence of the activity coefficient. The parameters α_a, α_c, and i_0^{ref}/C_{dl} were estimated as a function of SOC, and the results are shown in Figure 11 and Figure 12, respectively. The resulting values for the parameter i_0^{ref}/C_{dl} of the order of nV/s indicates a very large time constant for equilibration in this system (ca. 1 month). The estimated values for i_0^{ref}/C_{dl} are relatively constant with the SOC. Note that the estimated values of i_0/C_{dl} at any given state of charge depend on the value of the equilibrium potential at that SOC. For example, if the potentials at the end of the 10-hour relaxation period at 50% SOC are used as equilibrium potentials, the estimated values of i_0/C_{dl} are larger by an order of magnitude than those reported in Figure 12. The apparent transfer coefficient was fit to a linear relationship *versus* the SOC as given below

$$\alpha_a = 1.77z + 1.65$$
$$\alpha_c = 0.63z + 1.52 \quad [9]$$

These values agree very well with those estimated by Baggetto et al. (see Figure 9 in reference 79). The values of α_a and α_c are significantly higher than 0.5, indicating complex lithiation and delithiation reactions. Very large apparent transfer coefficients have been observed in some cases when the reactant is strongly solvated in a polar solvent.[88] In addition, as was pointed out before, stress effects[68,69] could also play a role during the open-circuit-potential behavior, modifying the nature of the potential evolution and contributing to the estimation of the apparent transfer coefficient as calculated in this study. A detailed model that incorporates the effect of stress based on theory developed by Bower et al. would further help in clarifying this issue.[89]

The open-circuit-potential-relaxation experiments were repeated during the first-cycle lithiation and delithiation in a PLD Si thin-film electrode as well as in amorphous Si thin-film electrodes. A 10-hour open-circuit-potential-relaxation experiment at various SOC intervals during the first lithiation of a PLD Si thin-film electrode is shown in Figure 13. The flat potential profile is a characteristic of solid-state amorphization of crystalline silicon upon lithiation.[12,74] The inset in this figure shows the open-circuit- potential evolution at 50% SOC after lithiation along with the model fit based on Equation 4. Between lithiation on a fresh PLD silicon thin-film electrode that is highly crystalline and on an amorphatized PLD silicon thin-film electrode, both the evolution of open-circuit potential as well as the estimated kinetic parameters do not vary, which indicates that they are intrinsic to lithiation and delithiation kinetics in silicon (i.e., the rate of electrochemical

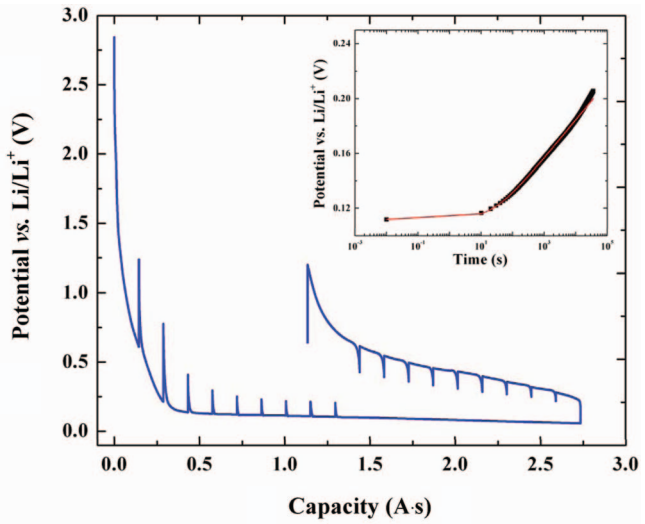

Figure 13. Potential vs. capacity for the first lithiation and delithiation between 1.2 and 0.01 V vs. Li/Li+ is shown along with ten-hour open-circuit-relaxation data at various intervals. The inset shows the open-circuit-potential evolution at ca. 50% SOC (based on charge consumed during initial lithiation) along with the model fit based on Equation 7.

Table I. Parameters used in the analysis of Li_xSi electrode.

Parameter	Value	Comments
A	2.54 cm^2	Measured
α_{side}	0.5	Assumed
C_{dl}	0.02 F/cm^2	Estimated[a]
F	96485 C/mol	Ref. 93
$i_{0,side}$	7.5×10^{-13} A/cm^2	Estimated[a]
i_0/C_{dl}	4.23 nV/s	Estimated
R	8.314 J/mol/K	Ref. 93
T	298 K	Measured
U_{side}	0.8 V vs. Li/Li^+	Assumed
V_c	3.8 V	Assumed

[a]Based on geometric area.

reactions and not the rate of phase transformation is limiting). A sample comparison between the estimated kinetic parameters at 50% SOC in crystalline and amorphous silicon thin-film electrodes is given in Table II. For sake of brevity, a detailed description of similar studies on amorphous Si thin-film electrodes with different electrolyte additives is not included here.

Closed-circuit simulation.— The estimated thermodynamic and kinetic parameters were then used to predict experimental data under other conditions. A closed-circuit experiment with neglect of the side reaction is described by the equation

$$I_{app} = C_{dl}\frac{dV}{dt} + i_0\left\{\exp\left[\frac{\alpha_a F}{RT}(V-U)\right] - \exp\left[-\frac{\alpha_c F}{RT}(V-U)\right]\right\} \quad [10]$$

Ohmic and diffusion losses are ignored because the total current is small. Equation 10 was solved numerically using a finite-difference routine, and Figure 14 shows the simulation results for $I_{app} = \pm 20.83\ \mu A/cm^2$. The parameters used for this simulation are listed in Table I. The model correctly predicts the potential offset during both lithiation and delithiation. The model does not predict the potential evolution on change in current (near z = 1), which requires a more accurate estimation of the capacitance. The model also deviates from features in the data seen at z = 0 and z = 0.6, both of which require a better open-circuit potential estimation. Figure 15 shows the simulation results corresponding to lithiation and delithiation at different rates. The apparent potentials for delithiation show a smaller spread with C rate than do those for lithiation similar to data shown in Figure 5. Also, the offset potential decreases with decrease in the lithiation/delithiation rate (Figure 16). This is not apparent in the data shown in Ref. 5 and in Figure 5 because the practical rates of lithiation/delithiation are within an order of magnitude whereas the decrease in the potential offset becomes significant if the lithiation/delithiation rates are decreased by four to five orders of magnitude. This is indicative of a system operating far away from equilibrium (i.e., in the Tafel regime) where the overpotential is fairly insensitive to the reaction rate. In conjunction with appropriate transport parameters, the equilibrium potential and the kinetic parameters reported here may be used in a continuum model to predict the electrochemical rate capability of the Li_xSi electrode.

Table II. Parameters estimated from open-circuit potential relaxation at 50% SOC from three different thin-film electrodes.

	PLD Si		Amorphous Si
Parameter	First cycle	Steady-state cycles	Steady-state cycles
$i_{0,a}/C_{dl}$	8.12 nV/s	2.77 nV/s	4.13 nV/s
α_a	1.93	1.95	2.14

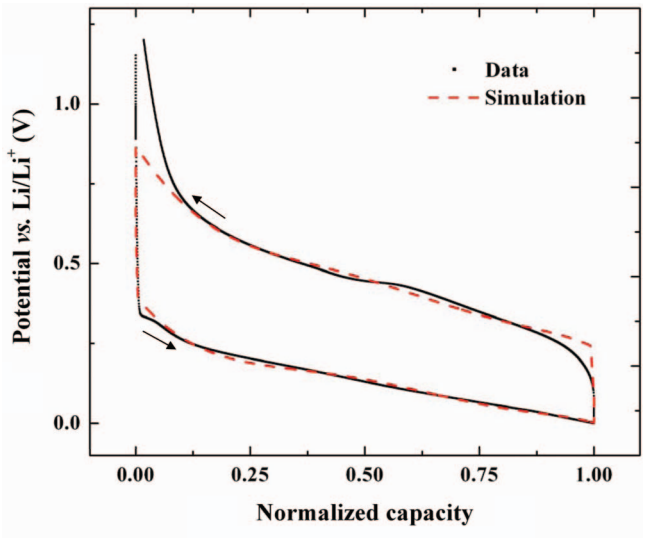

Figure 14. Simulation (dashed line) and data (points) corresponding to a constant current (Iapp = $\pm 20.83\ \mu A/cm^2$) lithiation and delithiation between 0 and 1.2 V vs. Li.

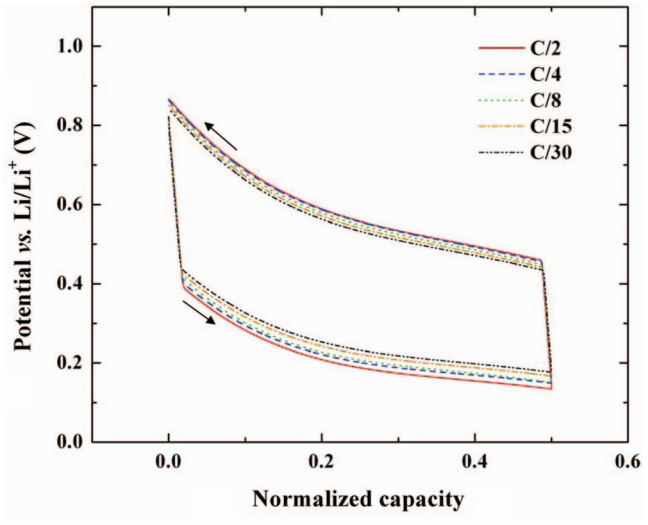

Figure 15. Simulated curves corresponding to different lithiation/delithiation rates ranging from C/2 to C/30. The offset potential decreases with decrease in the C rate.

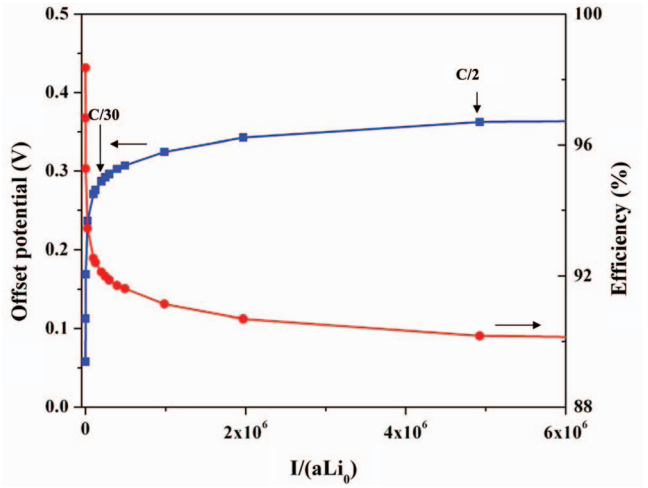

Figure 16. Combined potential offset (-■-) and percent efficiency (-●-) of lithiation/delithiation reactions for different C rates as predicted by the model.

Implications.— Cell efficiency for the Li_xSi/cathode system for a given SOC can be written as,

$$\%\,\text{Efficiency} = \left[1 - \frac{\left(V_c - V_a^l\right) - \left(V_c - V_a^d\right)}{\left(V_c - V_a^l\right)}\right] \times 100 \qquad [11]$$

where V_c is cathode potential, V_a^l and V_a^d are anode potentials vs. Li/Li^+ corresponding to lithiation and delithiation, respectively. The efficiency of the Li_xSi system approaches 100% as the offset between the lithiation and the delithiation reaction potentials (i.e., $V_a^d - V_a^l$) approaches 0. Figure 16 shows the predicted efficiency as a function of the ratio of lithiation/delithiation current to the exchange current density. A cathode potential of 3.8 V vs. Li/Li^+ was used for this calculation. For a C/10 rate, the model predicts approximately 91% energy efficiency. The minimum overall cell-level energy-efficiency goal set by the Office of Vehicle Technologies for power-assist hybrid electric vehicles is 90% on a load profile with variable rates.[90,91] USABC's long-term cell-level efficiency goal for advanced-battery technologies is 80% for a C/3 discharge followed by a 6-hour charge.[92] The model predicts that high energy efficiency could be obtained only by decreasing $I/(aLi_0)$ by five orders of magnitude. Since i_0 is an inherent property of the Li_xSi system, the potential offset cannot be removed, and an increase in efficiency could be achieved only by increasing the surface area of the electrode also by a factor of 10^5. However, increasing the surface area of the electrode would also increase the charge lost due to the formation of the SEI layer during the initial lithiation/delithiation cycle. The model also shows that high rates are possible despite having a potential offset.

Conclusions

The kinetics of lithiation and delithiation in silicon was studied on a model thin-film crystalline-silicon electrode. A Tafel equation (or a Butler-Volmer equation with a very small exchange current density) is shown to account for the irreversibility between lithiation and delithiation exhibited by a well cycled electrode. The potential hysteresis between the lithiation and delithiation reactions at any given SOC exhibited by the Li_xSi system is shown to be caused by a very large kinetic resistance (small i_0). In conjunction with a model based on Tafel kinetics and double-layer capacitance, data obtained from the open-circuit-relaxation experiments are used to estimate the apparent transfer coefficients and the ratio of exchange current density to double-layer capacitance, all as a function of SOC for both lithiation and delithiation reactions. With these parameters, the model is shown to predict successfully the behavior of the system under galvanostatic lithiation and delithiation. The model also predicts that high energy efficiency (or lowering the potential offset) could be obtained only by reducing $I/(aLi_0)$ by several orders of magnitude. In other words, a large increase in the surface area is required to enhance the energy efficiency of the silicon anodes. Overall, this simple model helps in understanding the limitations, and provides guidance to improving the performance of the Li_xSi system.

A methodology for correcting the cycling data for the side-reactions is presented. This allows for an accurate analysis of the cycling data and precise estimation of SOC of the active material in a well-cycled electrode. The side-reaction kinetic parameters explain the open-circuit-potential relaxation at longer time scales, where the potential evolution deviates from a Tafel-like behavior. On a well cycled-electrode, continuously occurring side-reactions is shown to cause the observed irreversible capacity loss in this system. This could possibly be due to the chemical or mechanical instability of the electrolyte-reduction products that constitute the SEI layer. Therefore, a more detailed understanding of the physical properties of the SEI layer is needed to arrest the side reaction and to minimize or eliminate the cycle-to-cycle capacity loss observed in this system. Also, more understanding about the structural changes between lithiation and delithiation is needed. The thermodynamic and kinetic parameters estimated in this study are currently being incorporated into a transport model to understand the true rate-capability limitations in this system.

Acknowledgments

The authors gratefully acknowledge the financial support from the Assistant Secretary for Energy Efficiency and Renewable Energy, Office of Vehicle Technologies, the United States Department of Energy under contract no. DE-AC02-05CH11231. The authors thank Dr. Robert Kostecki and Dr. Laurence J. Hardwick (LBNL) for help with Raman spectroscopy measurements; Xiaojun Zhang and Dr. Samuel S. Mao (LBNL) for help with pulse-laser deposition; Dr. Keith D. Kepler (Farasis Energy, Inc.) for help with coin-cell fabrication; Xiangyun Song (LBNL) for help with electron microscopy and X-ray measurements. The authors acknowledge the support of the National Center for Microscopy at LBNL, which is supported by the United States Department of Energy under contract no. DE-AC02-05CH11231. The authors acknowledge the Microlab at the Department of Electrical Engineering in the University of California, Berkeley, for the fabrication of amorphous Si thin films.

List of Symbols

C_{dl}	double layer capacitance, F/cm^2
I_{app}	applied current density, A/cm^2
i_0	exchange current density, A/cm^2
F	Faraday's constant, 96485 C/mol
L	film thickness, cm
T	temperature, K
t	time, s
U	equilibrium potential, V
V	potential, V
V_0	potential at time zero, V
V_c	cathode potential, V
V_a^l	anode potential corresponding to lithiation, V
V_a^d	anode potential corresponding to delithiation, V
z	State of charge

Greek

α_a	apparent transfer coefficient corresponding to delithiation
α_c	apparent transfer coefficient corresponding to lithiation
α_{side}	apparent transfer coefficient corresponding to the side reaction
λ	wavelength, nm
φ	diameter, cm

References

1. M. N. Obrovac and L. Christensen, *Electrochem. Solid State Letters*, **7**, A93 (2004).
2. J.-M. Tarascon and M. Armand, *Nature*, **414**, 359 (2001).
3. V. A. Sethuraman, L. J. Hardwick, V. Srinivasan, and R. Kostecki, *J. Power Sources*, **195**, 3655 (2010).
4. S. D. Beattie, D. Larcher, M. Morcrette, B. Simon, and J.-M. Tarascon, *J. Electrochem. Soc.*, **155**, A158 (2008).
5. C. K. Chan, H. Peng, G. Liu, K. McIlwrath, X. F. Zhang, R. A. Huggins, and Y. Cui, *Nature Nanotech.*, **3**, 31 (2008).
6. B. Gao, S. Sinha, L. Fleming, and O. Zhou, *Adv. Mater.*, **13**, 816 (2001).
7. K. Peng, J. Jie, W. Zhang, and S.-T. Lee, *Appl. Phys. Lett.*, **93**, 033105 (2008).
8. S. Bourderau, T. Brousse, and D. M. Schleich, *J. Power Sources*, **81-82**, 233 (1999).
9. A. Netz, R. A. Huggins, and W. Weppner, *J. Power Sources*, **119-121**, 95 (2003).
10. J. P. Maranchi, A. F. Hepp, and P. N. Kumta, *Electrochem. Solid State Letters*, **6**, A198 (2003).
11. V. Baranchugov, E. Markevich, E. Pollak, G. Salitra, and D. Aurbach, *Electrochem. Comm.*, **9**, 796 (2007).
12. P. Limthongkul, Y.-I. Jang, N. J. Dudney, and Y.-M. Chiang, *Acta Materialia*, **51**, 1103 (2003).
13. J. Graetz, C. C. Ahn, R. Yazami, and B. Fultz, *Electrochem. Solid State Letters*, **6**, A194 (2003).
14. M. N. Obrovac and L. J. Krause, *J. Electrochem. Soc.*, **154**, A103 (2007).
15. J. H. Ryu, J. W. Kim, Y.-E. Sung, and S. M. Oh, *Electrochem. Solid State Letters*, **7**, A306 (2004).

16. W.-R. Liu, M.-H. Yang, H.-C. Wu, S. M. Chiao, and N.-L. Wu, *Electrochem. Solid State Letters*, **8**, A100 (2005).
17. N. Dimov and M. Yoshio, *J. Power Sources*, **174**, 607 (2007).
18. M. K. Datta and P. N. Kumta, *J. Power Sources*, **158**, 557 (2006).
19. M. K. Datta and P. N. Kumta, *J. Power Sources*, **165**, 368 (2007).
20. N. Dimov, S. Kugino, and M. Yoshio, *Electrochim. Acta*, **48**, 1579 (2003).
21. U. Kasavajjula, C. Wang, and A. J. Appleby, *J. Power Sources*, **163**, 1003 (2007) and references therein.
22. S. Ohara, J. Suzuki, K. Sekine, and T. Takamura, *Electrochemistry*, **71**, 1126 (2003).
23. At 50% SOC in a cell made with pulse-laser deposited Si thin-film electrode and lithium metal counter and reference electrodes.
24. W.-R. Liu, Z.-Z. Guo, W.-S. Young, D.-T. Shieh, H.-C. Wu, M.-H. Yang, and N.-L. Wu, *J. Power Sources*, **140**, 139 (2005).
25. T. D. Hatchard and J. R. Dahn, *J. Electrochem. Soc.*, **151**, A838 (2004).
26. E. Peled, *J. Electrochem. Soc.*, **126**, 2047 (1979).
27. D. Aurbach, B. Markovsky, I. Weissman, E. Levi, and Y. Ein-Eli, *Electrochim. Acta*, **45**, 67 (1999).
28. D. Aurbach, Y. Talyosef, B. Markovsky, E. Markevich, E. Zinigrad, L. Asraf, J. S. Gnanaraj, and H. J. Kim, *Electrochim. Acta*, **50**, 247 (2004).
29. N. S. Choi, K. H. Yew, K. Y. Lee, M. Sung, H. Kim, and S. Kodambaka, *J. Power Sources*, **161**, 1254 (2006).
30. J. S. Gnanaraj, R. W. Thompson, J. F. DiCarlo, and K. M. Abraham, *J. Electrochem. Soc.*, **154**, A185 (2007).
31. Y. M. Lee, J. Y. Lee, H.-T. Shim, J. K. Lee, and J.-K. Park, *J. Electrochem. Soc.*, **154**, A515 (2007).
32. C. K. Chan, R. Ruffo, S. S. Hong, and Y. Cui, *J. Power Sources*, **189**, 1132 (2009).
33. S. P. V. Nadimpalli, V. A. Sethuraman, S. Dalavi, B. Lucht, M. J. Chon, V. B. Shenoy, and P. R. Guduru, *J. Power Sources*, **215**, 145 (2012).
34. N.-S. Choi, K. H. Yew, K. Y. Lee, M. Sung, and S.-S. Kim, *J. Power Sources*, **161**, 1254 (2006).
35. C. C. Nguyen and S.-W. Song, *Electrochim. Acta*, **55**, 3026 (2010).
36. V. Srinivasan, J. W. Weidner, and J. Newman, *J. Electrochem. Soc.*, **148**, A969 (2001).
37. E. Frackowiak, S. Gautier, H. Gaucher, S. Bonnamy, and F. Béguin, *Carbon*, **37**, 61 (1999).
38. B. Gao, A. Kleinhammes, X. P. Tang, C. Bower, L. Fleming, Y. Wu, and O. Zhou, *Chem. Phys. Lett.*, **307**, 153 (1999).
39. E. Frackowiak and F. Béguin, *Carbon*, **40**, 1775 (2002).
40. T. Zheng, W. R. McKinnon, and J. R. Dahn, *J. Electrochem. Soc.*, **143**, 2137 (1996).
41. M. Inaba, M. Fujikawa, T. Abe, and Z. Ogumi, *J. Electrochem. Soc.*, **147**, 4008 (2000).
42. J. S. Xue and J. R. Dahn, *J. Electrochem. Soc.*, **142**, 3668 (1995).
43. E. Buiel and J. R. Dahn, *Electrochim. Acta*, **45**, 121 (1999).
44. Q. Zhong, J. R. Dahn, and K. Colbow, *Phys. Rev. B*, **46**, 2554 (1992).
45. J. R. Dahn, U. von Sacken, and C. A. Michal, *Solid State Ionics*, **44**, 87 (1990).
46. A. Sawa, T. Fujii, M. Kawasaki, and Y. Tokura, *Appl. Phys. Lett.*, **85**, 4073 (2004).
47. A. Baikalov, Y. Q. Wang, B. Shen, B. Lorenz, S. Tsui, Y. Y. Sun, Y. Y. Xue, and C. W. Chu, *Appl. Phys. Lett.*, **83**, 957 (2003).
48. P. G. Bruce, A. R. Armstrong, and R. L. Gitzendanner, *J. Mater. Chem.*, **9**, 193 (1999).
49. G. Rousse, C. Masquelier, J. Rodríguez-Carvajal, and M. Hervieu, *Electrochem. Solid State Lett.*, **2**, 6 (1999).
50. N. J. Dudney, J. B. Bates, and F. X. Hart, *Meeting Abstracts* 96-2, Abstract No. 877, 190th Electrochemical Society Meeting, Oct. 6–11, 1996, San Antonio, TX.
51. S. H. Elder, L. H. Doerrer, F. J. DiSalvo, J. B. Parise, D. Guyomard, and J. M. Tarascon, *Chem. Mater.*, **4**, 929 (1992).
52. S.-C. Chin, H. Grondey, P. Strobel, M. Anne, and L. F. Nazar, *J. Am. Chem. Soc.*, **125**, 10402 (2003).
53. B. J. Neudecker, R. A. Zuhr, and J. B. Bates, *J. Power Sources*, **81-82**, 27 (1999).
54. V. Srinivasan and J. Newman, *Electrochem. Solid State Lett.*, **9**, A110 (2006).
55. J. L. Dodd, R. Yazami, and B. Fultz, *Electrochem. Solid State Lett.*, **9**, A151 (2006).
56. L. Y. Beaulieu, K. C. Hewitt, R. L. Turner, A. Bonakdarpour, A. A. Abdo, L. Christensen, K. W. Eberman, L. J. Krause, and J. R. Dahn, *J. Electrochem. Soc.*, **150**, A149 (2003).
57. W. Xing, A. M. Wilson, K. Eguchi, G. Zank, and J. R. Dahn, *J. Electrochem. Soc.*, **144**, 2410 (1997).
58. B. Villeret and M. Nechtschein, *Phys. Rev. Lett.*, **63**, 1285 (1989).
59. K. Meerholz and J. Heinze, *Electrochim. Acta*, **41**, 1839 (1996).
60. M. A. Vorotyntsev, E. Vieil, and J. Heinze, *J. Electroanal. Chem.*, **450**, 121 (1998).
61. H. He, J. Zhu, N. J. Tao, L. A. Nagahara, I. Amlani, and R. Tsui, *J. Am. Chem. Soc.*, **123**, 7730 (2001).
62. K. Aoki, J. Cao, and Y. Hoshino, *Electrochim. Acta*, **39**, 2291 (1994).
63. H. Y. Lee, W. S. Cho, S. M. Oh, H.-D. Wiemhöfer, and W. Göpel, *J. Electrochem. Soc.*, **142**, 2659 (1995).
64. Y. Jiang, S. Wang, Y. Zhang, J. Yan, and W. Li, *J. Electrochem. Soc.*, **145**, 373 (1998).
65. W. He, G. Lin, and T. V. Nguyen, *AIChE Journal*, **49**, 3221 (2003).
66. L. J. C. Jeuken and F. A. Armstrong, *J. Phys. Chem. B*, **105**, 5271 (2001).
67. M. D. Levi and D. Aurbach, *J. Phys. Chem. B*, **101**, 4630 (1997).
68. V. A. Sethuraman, M. J. Chon, M. Shimshak, V. Srinivasan, and P. R. Guduru, *J. Power Sources*, **195**, 5062 (2010).
69. V. A. Sethuraman, V. Srinivasan, A. F. Bower, and P. R. Guduru, *J. Electrochem. Soc.*, **157**, A1253 (2010).
70. V. A. Sethuraman, M. J. Chon, M. Shimshak, N. Van Winkle, and P. R. Guduru, *Electrochem. Comm.*, **12**, 1614 (2010).
71. J. P. Maranchi, A. F. Hepp, A. G. Evans, N. T. Nuhfer, and P. N. Kumta, *J. Electrochem. Soc.*, **153**, A1246 (2006).
72. V. A. Sethuraman, K. Kowolik, and V. Srinivasan, *J. Power Sources*, **196**, 393 (2011).
73. X. Y. Chen, Y. F. Lu, Y. H. Wu, B. J. Cho, and H. Hu, *MRS Symposium Proceedings*, **762**, A19.2.1 (2003).
74. M. J. Chon, V. A. Sethuraman, A. McCormick, V. Srinivasan, and P. R. Guduru, *Phys. Rev. Lett.*, **107**, 045503 (2011).
75. R. Darling and J. Newman, *J. Electrochem. Soc.*, **145**, 990 (1998).
76. K. P. Ta and J. Newman, *J. Electrochem. Soc.*, **145**, 3860 (1998).
77. V. L. Chevrier and J. R. Dahn, *J. Electrochem. Soc.*, **156**, A454 (2009).
78. J. Newman and K. E. Thomas-Alyea, *Electrochemical Systems*, 3rd ed., John Wiley & Sons, Inc., New York (2004).
79. L. Baggetto, R. A. H. Niessen, F. Roozeboom, and P. H. L. Notten, *Adv. Funct. Mater.*, **18**, 1057 (2008).
80. R. Chandrasekaran, A. Magasinski, G. Yushin, and T. F. Fuller, *J. Electrochem. Soc.*, **157**, A1139 (2010).
81. K. Yoshimura, J. Suzuki, K. Sekine, and T. Takamura, *J. Power Sources*, **174**, 653 (2007).
82. N. Ding, J. Xu, Y. X. Yao, G. Wegner, X. Fang, C. H. Chen, and I. Lieberwirth, *Solid State Ionics*, **180**, 222 (2009).
83. S. Davis, E. S. Takeuchi, W. Tiedemann, and J. Newman, *J. Electrochem. Soc.*, **154**, A477 (2007).
84. S. Davis, E. S. Takeuchi, W. Tiedemann, and J. Newman, *J. Electrochem. Soc.*, **154**, A477 (2007).
85. V. Srinivasan, G. Q. Wang, and C. Y. Wang, *J. Electrochem. Soc.*, **150**, A316 (2003).
86. B. Pillay and J. Newman, *J. Electrochem. Soc.*, **143**, 1806 (1996).
87. A. Constantinides and N. Mostoufi, *Numerical Methods for Chemical Engineers with MATLAB Applications*, pp. 439–481, Prentice Hall, Upper Saddle River, NJ (1999).
88. J. Lipkowski and P. N. Ross, pp. 357 ff., *Electrocatalysis*, WILEY-VCH (1998).
89. A. F. Bower, P. R. Guduru, and V. A. Sethuraman, *J. Mech. Phys. Solids*, **59**, 804 (2011).
90. FreedomCAR 42 V Energy Storage System End-of-Life Performance Goals, USCAR Electrochemical Energy Storage Technology Team, November 2002.
91. FreedomCAR Energy Storage System Performance Goals for Power Assist Hybrid Electric Vehicles, USCAR Electrochemical Energy Storage Technology Team, November 2002.
92. Electric Vehicle Battery Test Procedures Manual: Appendix G, USABC Criteria for Advanced Energy Technologies.
93. R. H. Perry and D. W. Green, *Perry's Chemical Engineer's Handbook*, 7th Edition, McGraw Hill (1997).